ABSTRACT

Title of Thesis: LEARNING AND ENHANCING IMPORTANT FLUCTUATIONS IN MODEL HAMILTONIAN SYSTEMS

Freddy Alexis Cisneros
Master of Science, 2019

Thesis directed by: Pratyush Tiwary, Dept. of Chemistry & Biochemistry

In this thesis, we discuss the need for enhanced sampling methods, namely to allow the simulation to sample hard to reach microstates of the system, allowing us to make better approximations of thermodynamic observables obtained from a simulation. To do this, we first introduce three enhanced sampling methods that can be applied Monte Carlo simulations with emphasis on the $2d$ Ising model. These three enhanced sampling methods are Wang-Landau sampling, a Variational Approach to Monte Carlo simulations developed by Yantao Wu and Roberto Car, and the Predictive Reweighted Autoencoded Variational Bayes for Enhanced Sampling (pRAVE) method which was developed by our group.

After introducing these three methods we then apply pRAVE to the $2d$ Ising model in the absence of an external magnetic field. Using pRAVE we explore the relative importance of the net magnetic moment to the average nearest neighbor interaction energy, and the average second nearest neighbor interaction energy as the critical temperature of the system T_C is approached. We compare our results to what we should expect given that the correlation length diverges as the critical temperature is approached. We also determine the heat capacity using data from our sim-

ulation to benchmarking against Onsager's asymptotic solution near the critical temperature T_C. We explain how discrepancies between Onsager's results and ours can be reduced by increasing the lattice size used in our analysis. We also provide free energy plots at temperatures ranging from $T = 0.9T_C$ to $T = 0.999T_C$ and show that the barrier separating the two states of the $2d$ Ising model decreases as the temperature T of the system is increased, in agreement with what should be observe.

After presenting our results, we discuss further work that can be done when applying pRAVE to the $2d$ Ising model as well as more complex Hamiltonians. This then paves the way for the use of pRAVE to study mechanisms for crystal nucleation as mentioned in the Conclusion of this thesis.

LEARNING AND ENHANCING IMPORTANT FLUCTUATIONS IN MODEL HAMILTONIAN SYSTEMS

by

Freddy Alexis Cisneros

Thesis submitted to the faculty of the Graduate School of the
University of Maryland, College Park in partial fulfillment
of the requirements for the degree of
Master of Science in Physics

2019

Advisory Committee:
Professor Pratyush Tiwary, Chair
Professor Christopher Jarzynski
Professor Edward Redish

Acknowledgements

I would like to everyone that made this journey possible. First, I would like to thank my mother Emma, my father Jesus, my sisters Leslie and Zulema, and my brother Jesse. If it weren't for your help I can't imagine any of this being possible. Thank you all for your patience when I was away from home studying over the years and always encouraging me to work harder and to never look back. The same goes to all of my aunts, uncles, and cousins who have greatly contributed to making this possible with their support all along the way. Whether the support was to help me overcome barriers when I felt I was at my lowest or whether it was in providing me a to stay when I was passing by your town, I know can always count on you. Also a big thank you to Natalia Ubilla for your endless help and support these past two years. I know that I can count on you at anytime for anything. The same goes to Mackenzie Flowers and Araseli Cortez who have been like a brother and sister to me during my time in college.

It often said that it takes a village to raise a child, and this has been very true for me. I don't think I would be here if it weren't for my community looking out for me as I was growing up. I can honestly say that it is because of my friends, their families that would take care of me when my parents worked endless nights what has given me the fuel to keep me going when I feel tired from studying. I hope I am making you all proud. For this I would like to give a special thanks all the families from Budlong Avenue and Marine, that have taken care of me and my brother when we were children. Thank you also to my childhood friends who I formed a brotherhood with where we would look after each other, anyone who knows where we grew up knows I am this old because of all these brothers looking after me. The experiences that we lived through have helped shaped me to the person I am today. I would therefore like to thank all of you, namely, Raymundo, Steven, Omar, Jr., Kevin, Miguel, Stevenson, Walter, Aaron, and everyone else from my neighborhood.

Getting to where I am in my studies today would also not be possible without the professors and academic advisors that have supported me with their help in deciding should go to pursue my dreams as well as by

writing me letters of recommendation. For this I thank Joshua Deutsch, Michael Dine, David Lederman all from the University of California, Santa Cruz. I would also like to thank Arturo Hernandez and Elizabeth Bermudez from El Camino College for all your help when applying to universities. Thank you all so much for your endless support over the years.

I'm also blessed to have been able to join so many research groups over the years from which I learned so many things. For this I would like to thank, Davy J. Kirkpatrick and Sergio Fajardo-Acosta for my research opportunity at Caltech during the summer of 2013, Marc F. Desrosiers for my research opportunity at NIST during the summer of 2014, David Williams for my research opportunity at the University of California, Santa Cruz during the summer of 2015. Dave Schuster and Jonathan Simon for my research opportunity at the University of Chicago during the summer of 2016, as well as Zack Schlesinger for allowing us to conduct research throughout my time at the University of California, Santa Cruz as well as Onuttom Narayan for allowing me to work with you to complete my senior thesis in 2017. Lastly but definitely not least, my current research group that has allowed me to conduct amazing research over the past year at the University of Maryland. I've learned an incredible amount of science in an incredibly short amount of time due to an amazing team. For this I would like to thank all of the group members that I've worked closely with, Pratyush Tiwary, Yihang Wang, Sun-Ting Tsai, Zachary Smith, João Marcelo Ribeiro, Debabrata Pramanik, and Shashwat Kapoor.

A big thank you to my defense committee as well, Pratyush Tiwary, Christopher Jarzynski, and Edward Redish. Thank you all for your patience and help!

List of Figures

List of Tables

Contents

Chapter 1

Introduction

When simulating physical processes such as a protein folding, a ligand binding/unbinding from a protein or even a particle under the influence of a potential $V(\vec{r})$, at finite temperature T, one often comes across the issue that the system will remain trapped in one of the many states of the system that are separated by an energy barrier [1,5,27,28]. If the barrier is much larger than the thermal fluctuations of the system, $E_{A\to B} >> k_B T$ (see Fig. 1.1),

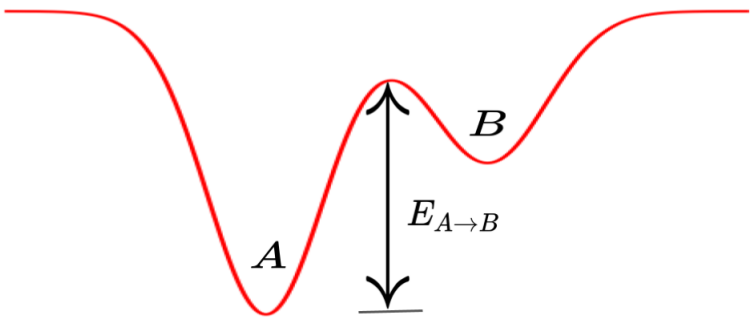

Figure 1.1: Two states A and B separated by an energy barrier $E_{A\to B} >> k_B T$ along an arbitrary axis.

then transitions between these two states will be unlikely to happen, as we will discuss in Sec. 2.1. To aid computer simulations in transitioning out of these trapped states, researchers have developed methods called "enhanced sampling methods" to allow the system to undergo such transitions through a variety of approaches [1-5,7,9,10,12,16,17,24]. Since the advent of such methods, a vast array of methods have been developed and continue to be developed to deal with both Molecular Dynamics (MD) simulations and Monte Carlo (MC) simulations. In this thesis we will discuss three such methods that are applied to MC simula-

tions, with an emphasis on the $2d$ Ising model. The main reason for this is to provide as much background material as possible for when we introduce the Predictive Reweighted Autoencoded Variational Bayes for Enhanced Sampling (pRAVE) method [5] developed in our group which is the core of this thesis.

In Chapter 2, we will review three enhanced sampling methods, namely, Wang-Landau sampling [7], a Variational Approach to Monte Carlo simulations developed by Yantao Wu and Roberto Car [12], and the Predictive Reweighted Autoencoded Variational Bayes for Enhanced Sampling (pRAVE) method [5]. In Chapter 3, we will apply pRAVE to the $2d$ Ising model in the absence of an external magnetic field. In Chapter 4, we will discuss how we can make further use of pRAVE on the $2d$ Ising model as well as other Hamiltonians similar to the $2d$ Ising model. However, before proceeding to describe enhanced sampling methods and how they're implemented let us first review the $2d$ Ising model as well as a few of the results that Onsager published in his 1943 paper for this model [19].

1.1 Ising Model

The Ising model that we will be considering is the $2d$ Ising model in the absence of an external magnetic field, Eq. 1.1, with periodic boundary conditions (PBC). We consider PBC as opposed to fixed boundary conditions due to the vast amount of numerical results and methods that have been proposed which allow us to compare the performance of our method. By applying PBC to the $2d$ Ising model, we can also benchmark our numerical results to Onsager's results, Sec. 1.2, which were obtained by considering a rectangular lattice with a large number of lattice sites, $N \to \infty$. Let us begin by summarizing this model.

The energy of the system that we will be considering will be the nearest neighbor interaction energy, Fig. 1.2, which is computed using the following Hamiltonian,

$$H = -J \sum_{i,j} \sigma_{i,j}[\sigma_{i+1,j} + \sigma_{i-1,j} + \sigma_{i,j+1} + \sigma_{i,j-1}], \tag{1.1}$$

where $\sigma_{i,j} \in \{+1, -1\}$ and $J = 1$. We will also set k_B to 1 when running simulations. We are considering this isotropic case as it will allow us to observe critical behavior near the critical temperature where $k_B T_C/J \approx 2.269$ that we can benchmark against Onsager's results [13].

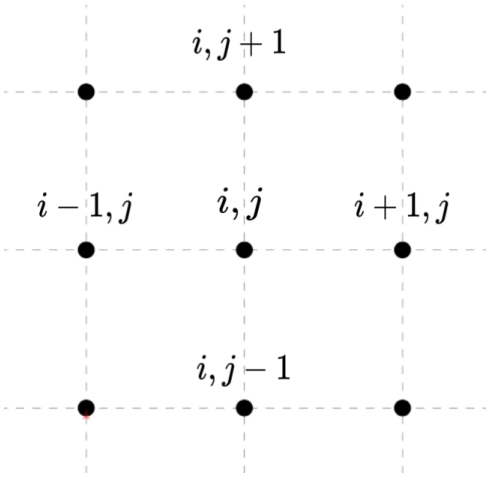

Figure 1.2: Portion of the lattice labeling the nearest neighbor spins that the spin $\sigma_{i,j}$ interacts with.

For an $L \times L$ lattice with N lattice sites such as the one that we are considering, the number of microstates of the systems is 2^N. Even for a small lattice of size 25×25 it is impossible to sample all $2^{625} \approx 10^{188}$ microstates in a simulation to compute the partition function, and from this thermodynamic observables. We must therefore develop a method to approximate the partition function by allowing us to visit more microstates of the system. This is where enhanced sampling comes into the picture. However, before discussing enhanced sampling methods let use first review the analytical results that Lars Onsager derived in his 1943 paper [19].

1.2 Analytical Results

Here we present Onsager's results for the $2d$ Ising model in the absence of an external magnetic field. It should be noted that even though Onsager's original paper [19] was published almost 80 years ago, these results continue to be the main source to benchmark numerical methods that can be applied to discrete Hamiltonians [11,12,16-18]. Onsager's solution of the $2d$ Ising model allowed him to derive an expression for the partition function, Eq. 1.2, by making use of rather laborious methods. In these methods he called upon various sub-branches of Algebra, such as Group Theory and Representation Theory, when building the problem of a rectangular lattice from $1d$ lattice chains. Onsager also called upon Hyperbolic Trigonometry when solving the Eigenwert problem to derive the partition function in Eq. 1.2. Rather than going through this treacherous yet scenic route, we present here Onsager's solution for the partition function from which other thermodynamic observables can be derived from,

$$Z = [2\cosh(\beta J)e^{I}]^N, \tag{1.2}$$

where β is the inverse temperature, N is the number of lattice sites and I is the following elliptic integral,

$$I = \frac{1}{2\pi}\int_0^\pi d\phi \ln\{\frac{1}{2}[1+(1-\kappa^2\sin^2\phi)^{1/2}]\}, \tag{1.3}$$

where $\kappa = 2\sinh(2\beta J)/\cosh^2(2\beta J)$. From this partition function, we can get other thermodynamic observables such as entropy,

$$S = \frac{\partial}{\partial T}(k_B T \ln Z), \tag{1.4}$$

the average energy of the system,

$$\langle E\rangle = k_B T^2 \frac{\partial \ln Z}{\partial T} \tag{1.5}$$

and the heat capacity of the system,

$$C = \frac{\partial\langle E\rangle}{\partial T} = \frac{\partial^2 \ln Z}{\partial \beta^2}. \tag{1.6}$$

In Ch. 3, we will be comparing our results for the heat capacity to Onsager's asymptotic approximation of the heat capacity near the critical temperature T_C,

$$C \sim -\left(\frac{8k_B N}{\pi}\right)(\beta J)^2 \ln|T - T_C|. \tag{1.7}$$

It is important to note an effect that arises near T_C that becomes an issue when running simulations around this temperature. Given that the system has an energy minimum when all the spins align, there is a tendency for spins to influence each other into aligning. This tendency is observed in computing the correlation function and as T_C is approached the correlation length increases. This makes it possible for spins that are far apart to influence each other. Therefore, since the spins want to align with one another and there is also a long range correlation length the system will transition back and forth between all the spins pointing up and all spins pointing down when a single spin flips at random. This effect where all the spins point up then quickly transition to all spins point down makes it difficult to sample intermediate configurations, configurations where there is a mixture of spins pointing up and others pointing down. Therefore, if our goal in using a simulation is to sample all possible spin configurations in order to compute the partition function, we will need an enhanced sampling method to encourage the system to sample these intermediate spin configurations. In the following chapter we will discuss several enhanced sampling methods that can be applied to the $2d$ Ising model, including pRAVE which we introduce in Sec. 2.4 and apply to this model in Ch. 3.

Chapter 2

Enhanced Sampling Methods

2.1 Notation and Definitions

The notation that we will be using throughout this paper is defined in the following as it makes it easy to discuss the enhanced sampling methods in Sec. 2.2 to 2.4*.

Microstates of a Physical System

Consider a physical system with a set of $\hat{\Omega}$ microstates which we will denote as,

$$\Omega = \{X_i : i = 1, 2, \cdots, \hat{\Omega}\} \tag{2.1}$$

and their associated probabilities,

$$\{p(X_i) : i = 1, 2, \cdots, \hat{\Omega}\}, \tag{2.2}$$

where X_i is the ith microstate. The probabilities in Eq. 2.2 may represent the probabilities of a system in thermal equilibrium with a heat reservoir at an inverse temperature of $\beta = 1/k_B T$ such that,

$$p(X_i) = \frac{1}{Z} \exp[-\beta E(X_i)], \text{ where } Z = \sum_{i=1}^{\hat{\Omega}} \exp[-\beta E(X_i)]. \tag{2.3}$$

Now that we have the notation that is necessary to discuss the enhanced sampling methods, we can proceed to discuss the Metropolis algorithm which allows us to transition from one microstate to the next using the probabilities given in Eq. 2.3.

*This notation was inspired by [7].

Sampling Microstates Using The Metropolis Algorithm

Suppose that we wish to sample a chain of microstates such as,

$$X_0(\in \Omega) \to X_1(\in \Omega) \to \cdots \to X_i(\in \Omega) \to X_{i+1}(\in \Omega),$$

where each microstates has a probability $p(X_i)$ of occurring. One way to construct such a chain is by making use of the Metropolis algorithm which is defined as follows: Suppose that we initialize our system under some arbitrary set of conditions and that the system is currently in microstate X_i with a corresponding energy $E(X_i)$. In order to transition to a microstate X_{i+1} we first make a small and random change to the system to obtain a trial microstate X_t with an energy $E(X_t)$. We determine whether or not to set this trial microstate as the microstate X_{i+1} by first computing the change of energy difference $\Delta E = E_t - E_i$. If this change of energy in transitioning from X_i to X_t is less than zero then we set X_{i+1} to X_t. We do this because we are simulating a physical process, and we know that a physical system always wants tends to the lowest energy state possible. However, we also want to allow random thermal fluctuations to occur which may not be energetically favorable, $\Delta E > 0$.

To allow random thermal fluctuations to occur when $\Delta E > 0$ we first need compute the probability of making such a transition. This can be done by computing the transition probability p which is given by,

$$p = \min\,(1, p_t/p_i) = \min\,(1, \exp\{-\beta \Delta E\}). \tag{2.4}$$

To decide whether we set X_{i+1} to X_t or X_i we make use of a random number generator that generates a float c between 0 and 1. If $c < p$ we allow the system to transition to the trial microstate, we set X_{i+1} to X_t. If $c > p$ we will stay in our current microstate, we set X_{i+1} to X_i.

One thing to note here is that the probability of transitioning from X_i to X_t decreases as the energy difference, ΔE, between these two microstates increases. This means that when we perform a simulation using the Metropolis algorithm, the system will want to tend towards a local energy minimum and will fluctuates about this minimum. This also suggests that if we wish to transition from one state to another that are separated by a large energy barrier, e.g. state A and B separated by an energy barrier, $E_{A\to B} >> k_B T$, as shown Fig. 1.1, this may require a large amount of computational time before such a transition occurs. To encourage the system in making such a transition, without having to increase the temperature of the system, requires the use of enhanced sampling methods such as the following.

2.2 Wang-Landau Sampling

The Wang-Landau algorithm [7,18] is a popular enhanced sampling method that is commonly used to estimate the density of states, $g(E)$, of a system after applying this algorithm to several iterations of MC simulations. This method makes use of a histogram, $H(E)$, that counts the number of times a macrostate E has been sampled and updating a function $g(E)$ that is inversely proportional to the probability, $p(E)$ every time the macrostate E is sampled. It is this update of $g(E)$ what encourages the system to visit macrostates that were not frequently visited, and what makes this algorithm an enhanced sampling method.

One significance of knowing $g(E)$ is that this allows us to reduce having to compute the partition function,

$$Z = \sum_i e^{-\beta E_i}, \tag{2.5}$$

to having to compute,

$$Z = \sum_E g(E) e^{-\beta E}. \tag{2.6}$$

Both partition functions are equal to each other, however, the partition function in Eq. 2.5 usually has many more terms to sum over than the partition function in Eq. 2.6. The reason for this is that Eq. 2.5 sums over microstates while Eq. 2.6 sums over the macrostates.

To apply the Wang-Landau algorithm we first initialize a histogram $H(E) = 0 \; \forall \; E$. We also initialize a function $g(E) = 1 \; \forall \; E$. Now that our histogram $H(E)$ and function $g(E)$ have been initialized it is time to initialize the system under some arbitrary set of conditions. e.g. we might want to initialize our lattice such that the average magnetic moment is approximately zero at the beginning of the simulation. Now that all the necessary initializations have been made, we can now go through the algorithm in detail.

Suppose that at the beginning of the simulation we are in microstate X_i with an energy $E(X_i)$. The first thing we must do is perform the following updates, $g(E_i) = \alpha \times g(E_i)$ and $H(E_i) = H(E_i) + 1$. In the first MC Simulation $\alpha = e^1 \approx 2.718$, however, in subsequent MC simulations we will update the function $g(E)$ using a modified factor α which we will soon discuss. Now that we have performed these updates, we make a small and random change to system to obtain a trial microstate X_t with energy an energy $E(X_t)$. However, unlike the Metropolis algorithm where we made a decision to transition from X_i to X_t based on a probability that depended on the energy difference, $\Delta E = E_t - E_i$, we now make a decision based on the

ratio $g(E_i)/g(E_t)$, such that probability p to transition from X_i to X_t becomes,

$$p = \min\,(1, p_t/p_i) = \min\,(1, g(E_i)/g(E_t)). \tag{2.7}$$

As mentioned at the beginning of this section, $p(E_i) \propto 1/g(E_i)$ and $p(E_t) \propto 1/g(E_t)$. Using a random number generator we generate a float c between 0 and 1, if $c < p$ then we make the transition from X_i to X_t. However, now along with setting X_{i+1} to X_t we also make the following updates, $g(E_t) = \alpha \times g(E_t)$ and $H(E_t) = H(E_t) + 1$. If on the other hand $c > p$, then we set X_{i+1} to X_i and we make the following updates, $g(E_i) = \alpha \times g(E_i)$ and $H(E_i) = H(E_i) + 1$.

We continue building our chain of microstates,

$$X_0(\in \Omega) \to X_1(\in \Omega) \to \cdots \to X_i(\in \Omega) \to X_{i+1}(\in \Omega),$$

this way until the histogram $H(E)$ has more or less flattened, meaning that all the bins of the histogram $H(E)$ are no less than a preset percentage of the histogram average, $\langle H(E)\rangle$. Once this condition has been met we prepare a new MC simulation by re-initializing the system. We also re-initialize the histogram, $H(E) = 0\ \forall\ E$. However, we keep the values $g(E)$ from the previous simulation which we will continue updating in this new simulation. In this new simulation we will also multiply $g(E)$ by a different factor, namely $\alpha \to \sqrt{\alpha} = e^{1/2}$. At the end of each MC simulation we continue updating the factor $\alpha \to \sqrt{\alpha}$ for the next MC simulation. We continue this process of running MC simulations and terminating them once the histograms have "flattened", as well updating the function $g(E)$ until the updating factor α does not change by an appreciable amount. In the following table we see the updating factors α that will be used for the nth MC simulation,

MC simulation	α
1	1
5	$1 + 6 \times 10^{-2}$
10	$1 + 2 \times 10^{-3}$
15	$1 + 6 \times 10^{-5}$
20	$1 + 2 \times 10^{-6}$
25	$1 + 6 \times 10^{-8}$
30	$1 + 2 \times 10^{-9}$

Table 2.1: α values that will be used for the nth MC simulation.

From Table 2.1 we see that the function $g(E)$ will not change by an appreciable amount after the 25th MC

simulation, we can therefore stop running MC simulations after the 24th simulation.

After applying this method to many MC simulations the function $g(E)$ will converge to the density of states for the system we are analyzing. The success of this method can be seen in Fig. 2.1 where Landau et al. accurately determined the density of states for the $2d$ Ising model using a 16×16 lattice and where they stopped running new MC simulations when α became less than $\exp\{10^{-8}\}$. From this analysis they also obtained accurate results of thermodynamic observables as detailed in their paper [17].

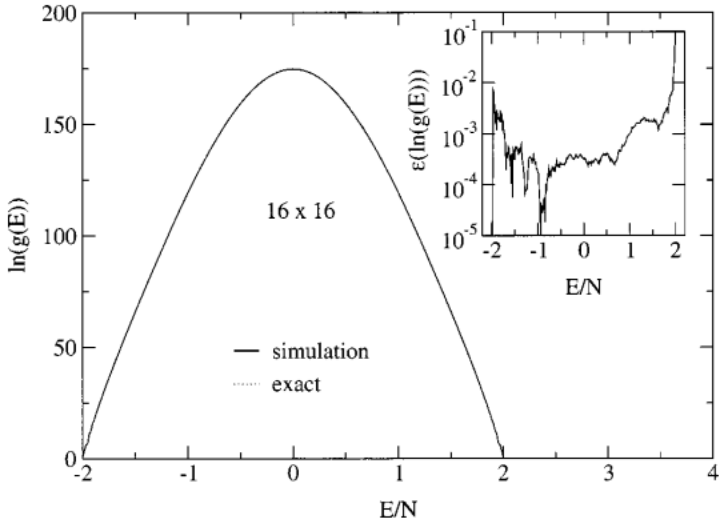

Figure 2.1: $\ln g(E)$ vs. E/N for a lattice of size 16×16 [17].

2.3 Variational Approach to Monte Carlo Simulations

Another enhanced sampling method that can be applied to the $2d$ Ising model is a method recently developed by Yantao Wu and Roberto Car [12]. This method works to eliminate the critical slow down of MC updates that arises from the divergence of the correlation length near T_C, as was explained in Sec. 1.2. This method makes use of a functional, $\Omega[V]$, that was introduced by Omar Valsson and Michele Parrinello in [4] which allows one to construct a bias potential that minimizes this functional $\Omega[V]$, and by construction allows one to eliminate the critical slow down of MC updates.

We introduce Wu and Car's enhanced sampling method by reviewing their use of the method to compute the renormalized coupling constants for the $2d$ Ising model in the absence of an external magnetic field [12]. To begin, let us consider the generic form of the $2d$ Ising model Hamiltonian,

$$H(\sigma) = \sum_{\alpha} K_{\alpha} S_{\alpha}(\sigma), \tag{2.8}$$

where the K_α's are coupling constants and the S_α's are classical operators that act on the spins to produce spin products and sums. Consider also a scale transformation, $\sigma' = \tau(\sigma)$, that coarse grains the lattice, such as a Kadanoff transformation [11] (see Fig. 2.2).

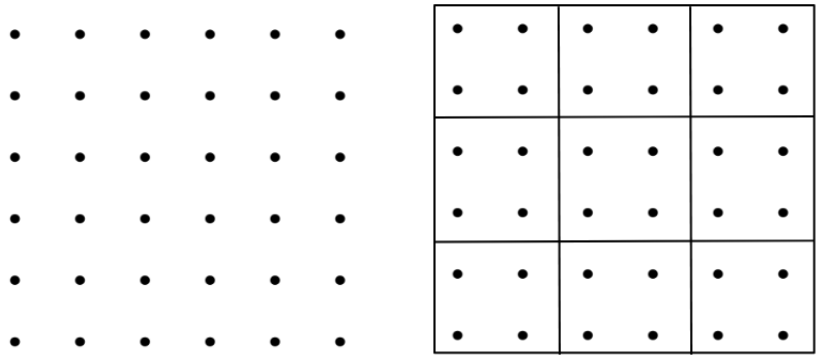

Figure 2.2: (Left) Original lattice. (Right) Lattice from the left after applying a Kadanoff block transformation where we have reduced the original $L \times L$ lattice to a $L/3 \times L/3$ lattice.

This coarse-graining effect then produces the following probability distribution relationship,

$$p(\sigma') = \frac{\sum_\sigma \delta(\sigma' - \tau(\sigma)) e^{-H(\sigma)}}{Z} = \frac{e^{-H'(\sigma')}}{Z'} \tag{2.9}$$

where,

$$Z = \sum_\sigma e^{-H(\sigma)} = \sum_{\sigma'} e^{-H'(\sigma')} = Z' \tag{2.10}$$

and where,

$$H'(\sigma') = -\log \sum_\sigma \delta(\sigma' - \tau(\sigma)) e^{-H(\sigma')}. \tag{2.11}$$

It is important to note that the inverse temperature β does not appear here since it is absorbed in the coupling constants K_α, e.g. in the isotropic case discussed in Sec. 1.1 K would be equal to βJ.

As mentioned in Sec. 1.2, there is a critical slow down the arises from the divergence of the correlation length near T_C. To get rid of this critical slow down, Wu and Car introduced a bias potential $V(\sigma')$ which forces the biased block spin probability distribution, $p_V(\sigma')$, to be equal to a chosen target distribution, $p_t(\sigma')$, such as a uniform probability distribution. This uniform probability distribution gives every "block lattice site" the same probability, thereby eliminating correlation effects.

To do this Wu and Car made use of a functional of the bias potential, $\Omega[V]$, that was introduced in [4].

Applying $\Omega[V]$ to this system we get,

$$\Omega[V] = \log \frac{\sum_{\sigma'} e^{-[H'(\sigma')+V(\sigma')]}}{\sum_{\sigma'} e^{-H'(\sigma')}} + \sum_{\sigma'} p_t(\sigma')V(\sigma'), \tag{2.12}$$

where $p_t(\sigma')$ is the target probability distribution. $\Omega[V]$ has the interesting property that it is a convex functional with a minimum at $V_{min}(\sigma')$ that is determined by,

$$H'(\sigma') = -V_{min}(\sigma') - \log p_t(\sigma') + \text{const.} \tag{2.13}$$

The probability distribution for σ' when using the bias potential $V_{min}(\sigma')$ then becomes,

$$p_{V_{min}(\sigma')} = \frac{e^{-\beta[H'(\sigma')+V(\sigma')]}}{\sum_{\sigma'} e^{-\beta[H'(\sigma')+V(\sigma')]}} = p_t(\sigma'), \tag{2.14}$$

To determine an approximation for the bias potential $V(\sigma')$ that minimizes the functional $\Omega[V]$ we first approximate $V(\sigma')$ using $V_{\mathbf{J}}(\sigma')$, a linear combination of a finite number of S_α terms with unknown coefficients J_α that form a vector $\mathbf{J} = \{J_1, J_2, \cdots, J_n\}$, and that we need to determine. We can then determine these coefficients using the gradient and Hessian which give us,

$$\frac{\partial \Omega(\mathbf{J})}{\partial J_\alpha} = -\langle S_\alpha(\sigma')\rangle_{V_{\mathbf{J}}} + \langle S_\alpha(\sigma')\rangle_{p_t}, \tag{2.15}$$

and

$$\frac{\partial^2 \Omega(\mathbf{J})}{\partial J_\alpha J_\beta} = -\langle S_\alpha(\sigma')S_\beta(\sigma')\rangle_{V_{\mathbf{J}}} + \langle S_\alpha(\sigma')\rangle_{V_{\mathbf{J}}}\langle S_\beta(\sigma')\rangle_{V_{\mathbf{J}}}, \tag{2.16}$$

where $\langle\cdot\rangle_{V_{\mathbf{J}}}$ is the biased ensemble average under $V_{\mathbf{J}}$ and $\langle\cdot\rangle_{p_t}$ is the ensemble average performed over the target probability distribution p_t.

One amazing note about this method is that this method allows us to approximate the renormalized Hamiltonian $H'(\sigma')$ by,

$$H'(\sigma') = -V'_{min}(\sigma') = -\sum_\alpha J_{\min,\alpha} S_\alpha(\sigma'), \tag{2.17}$$

which allows us to obtain an approximation for the renormalized coupling constants since,

$$K'_\alpha = -J_{\min,\alpha}. \tag{2.18}$$

By approximating the renormalized Hamiltonian $H'(\sigma')$ by using a linear combination of classical spin

operators, S_α that act on the spins we can determine the relative importance of an operator if we determine that magnitude of the coefficient, $J_{\min,\alpha}$, for one operator is smaller in magnitude than the rest of the operators, as mentioned in [12].

2.4 Predictive Reweighted Autoencoded Variational Bayes for Enhanced Sampling (pRAVE)

Here we present the Predictive Reweighted Autoencoded Variational Bayes for Enhanced Sampling method (pRAVE) [5] which is an enhanced sampling method that makes use of the Predictive Information Bottleneck (PIB) [21,22]. The motivation behind PIB and pRAVE is in finding the minimalist representation of the system's past, using the system's previous trajectory, that will allow us to make accurate predictions of the system's future. In the example that we will consider in Ch. 3, we will be mapping our dataset $X \in \mathbb{R}^3$ to a low-dimensional manifold $\chi \in \mathbb{R}$, that by construction will be the reaction coordinate for the system. This low-dimensional manifold will then be used to reconstruct our dataset $X' \in \mathbb{R}^3$. This training of the deep neural network shown in Fig. 2.3 that allows pRAVE to learn the reaction coordinate χ that best describes the system is only a small demonstration of the powers of pRAVE. In the following we will discuss describe the way that pRAVE works as well as the ability for pRAVE to learn a low-dimensional manifold χ that allows pRAVE to make accurate predictions of the systems future.

To explain how pRAVE works suppose that we have a high dimensional dataset X_t* that was taken at some time t and that characterizes the state of the system under some generic thermodynamic set of conditions, e.g. this dataset can be the trajectory of an N particle system in three-dimensional space in which case $X_t \in \mathbb{R}^{3N}$. Suppose further that we wish to predict information $X_{t+\Delta t}$ about the system at some time $t + \Delta t$ after the dataset X_t was recorded. We will make the assumption that X_t and $X_{t+\Delta t}$ are related through the conditional probability $P(X_{t+\Delta t}|X_t)$. The mutual information $I(X_t, X_{t+\Delta t})$ then quantifies the amount of information that an observation at time t tells us about an observation at some later time $t + \Delta t$. Additionally we will restrict our attention to a stationary process in the sense that the origin of time t is irrelevant, the importance then lies in the size of Δt. For this reason we will choose to represent our datasets X_t and $X_{t+\Delta t}$ as X and $X_{\Delta t}$ respectively. The principle of the PIB postulates that the "bottleneck" χ is related to the signal X through an encoder function $P(\chi|X)$. With this bottleneck χ we can predict information $X_{\Delta t}$ about the system's future by making use of a stochastic deep neural network

*Here, as well as in the rest of this section, the subscripts t and $t + \Delta t$ are used to denote the time that a dataset was recorded rather than a data point, X_i.

which we use as our decoder $P(X_{\Delta t}|\chi)$ as shown in Fig. 2.3.

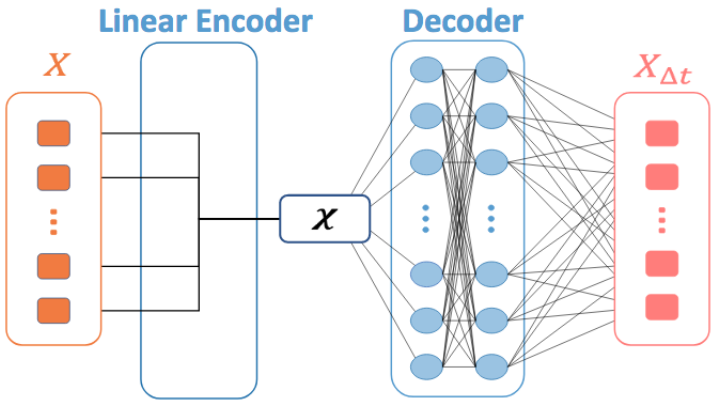

Figure 2.3: Architecture of pRAVE that is used to learn the PIB, χ.

The decoder used in pRAVE is a two layer stochastic deep neural network with 128 neurons on each layer.

This process of predicting the future with minimal amount information falls into the form of an optimization problem. We can express this problem as the optimization of the objective function $\mathcal{L}$ which is the difference between the two mutual informations $I(\chi, X_{\Delta t})$ and $I(X, \chi)$ which quantifies the amount of information that χ tells us about $X_{\Delta t}$ and amount of information that X tells us about χ respectively, namely

$$\mathcal{L} \equiv I(\chi, X_{\Delta t}) - \gamma I(X, \chi). \tag{2.19}$$

The objective function, $\mathcal{L}$, therefore quantifies the trade-off between complexity and the prediction through the parameter $\gamma \in [0, \infty)$.

The encoder $P(\chi|X)$ and decoder $P(X_{\Delta t}|\chi)$ can be implemented many ways [1, 18, 21], however, in the present work we will make use of a simple deterministic encoder $P(\chi|X)$ and a stochastic deep neural network as our decoder $P(X_{\Delta t}|\chi)$. The advantage of using a simple linear encoder is that this allows pRAVE to learn an information bottleneck, that is physically interpretable as the reaction coordinate χ of the system, which is difficult to achieve in machine learning. Introducing a simple linear encoder also allows us to drop the complexity term in Eq. 2.19, $\gamma = 0$, thereby simplifying our objective function to,

$$\mathcal{L} = I(\chi, X_{\Delta t}). \tag{2.20}$$

We will now work on optimizing $\mathcal{L}$ and developing a method where we can use this objective function

for enhanced sampling. To do this we will take inspiration from [1] which makes it possible for us to use Eq. 2.20 iteratively for enhanced sampling through a series of simulations that are progressively biased using importance sampling, while at the same time learning an increasingly accurate PIB. To see how, first imagine that we run an unbiased simulation and obtain the trajectory $X = \{X_1, X_2, \cdots, X_M\}$ of the system, which is M data points living in some high dimensional space. Using this dataset we want to find a low-dimensional mapping from X to χ that maximizes $\mathcal{L}$. At the heart of this is Bayes' theorem, $P(X_{\Delta t}|\chi)$, which we will see shortly. However, using Bayes' theorem can become impractical as the dimensionality of the dataset X becomes large [18]. One way to get around this issue is by making use of the principle of variational inference [25] which we now discuss: Consider the probability $P_\theta(\chi|X)$ where θ is a set of parameters that parameterize the PIB, such as a, b, and c in Eq. 3.4. What we hope to do is find the optimal low dimensional representation χ, or equivalently, the encoder parameters θ,

$$\theta = \arg\max_\theta \mathcal{L}(\theta), \tag{2.21}$$

that optimizes the PIB. Even though this optimization problem is intractable when the dimensionality of X is large, we can transform this into an approximate inference problem by making use of an approximate decoder $Q_\Phi(X_{\Delta t}|\chi)$ which is parameterized by Φ. In the case of pRAVE this corresponds to the weights to the deep neural network in Fig. 2.3. The mutual information in Eq. 2.20 can then be written as,

$$I(\chi, X_{\Delta t}) = H(P(X_{\Delta t})) - H(P_\theta(X_{\Delta t}|\chi)) \geq H(P(X_{\Delta t})) - C(P_\theta(X_{\Delta t}|\chi)||Q_\Phi(X_{\Delta t}|\chi)), \tag{2.22}$$

where H and C are the Shannon and cross entropy respectively and we have made use of Gibbs' inequality. Given that $H(P(X_{\Delta t}))$ is independent of our model parameters, θ and Φ, we can ignore this term in the optimization, thereby yielding a lower bound for the objective function,

$$\mathcal{L} \geq -C(P_\theta(X_{\Delta t}|\chi)||Q_\Phi(X_{\Delta t}|\chi)) = \mathcal{L}', \tag{2.23}$$

which is a tractable lower bound. This objective function also lends itself to a simple physical interpretation since we are trying to make Q have the same probability distribution as P in predicting $X_{\Delta t}$ given knowledge of χ. Therefore, by maximizing the right hand side of Eq. 2.23 in terms of the encoder/decoder parameters θ and Φ we are in effect solving the optimization problem that we set out to solve. The way we maximize $\mathcal{L}'$ in practice is the following: Suppose you have a large dataset with $M + k$ data points $\{X_1, X_2, \cdots, X_{M+k}\}$ and using the parameters θ, $\theta = (a, b, c)$ in the case of Eq. 3.4, we map this trajectory onto χ such that we

form a set $\chi = \{\chi_1, \chi_2, \cdots, \chi_{M+k}\}$. With these two datasets, χ and X, we can then compute $\mathcal{L}'$ since,

$$\mathcal{L}' = -C(P_\theta(X_{\Delta t}|\chi)||Q_\Phi(X_{\Delta t}|\chi)) = \int\int P_\theta(X_{\Delta t}|\chi)\ln Q_\Phi(X_{\Delta t}|\chi)dX_{\Delta t}d\chi = \frac{1}{M}\sum_{n=1}^{M} Q(X_{n+k}|\chi_n), \quad (2.24)$$

where χ_n is sampled from $P(\chi|X_n)$ and the simulation "time interval" between X_n and X_{n+k} is Δt. The way that we compute the log-likelihood in Eq. 2.24 is by using the mean squared error when training the neural network, as is outlined in pg. 130 of [18].

As mentioned earlier, most systems of interest will contain many states where the system may remain trapped in during an unbiased simulation. Therefore, the current PIB will represent the best estimate for the PIB of the system which we can use to perform importance sampling of the energy landscape. We do this by constructing a bias potential $V_{bias}(\chi)$ by mapping our trajectory X onto the PIB, χ using the parameters θ that optimized the objective function $\mathcal{L}'$. Once we have mapped the dataset X to χ we construct the following probability distribution,

$$P(\chi) = \langle\delta(\chi_- \chi(t))\rangle, \quad (2.25)$$

by binning and normalizing χ. We then use this probability distribution to construct the following bias potential,

$$V_{bias}(\chi) = k_B T \ln P(\chi) = k_B T \ln\langle\delta(\chi - \chi(t))\rangle. \quad (2.26)$$

What this bias potential will serve to do in the following simulation encourage the system to visit microstates that have not are not frequently sampled.

An application of this method of enhanced sampling is given in the following chapter where we apply pRAVE to the $2d$ Ising model. In that example the PIB is the reaction coordinate by construction and is chosen to be,

$$\chi = aS_1 + bS_2 + cS_3, \quad (2.27)$$

where S_1, S_2, S_3 are order parameters, namely the net magnetic moment, the average nearest neighbor interaction energy, and average second nearest neighbor interaction energy of a lattice configuration.

However before moving on to Ch. 3, we must point out that in performing multiple iterations of importance sampling we will need to perform reweighting to remove the effect of the biasing. This must be done so that we can compute the correct thermodynamics of the system. How we perform reweighting to undo

the biasing effect when constructing the bias potential will be given in the following chapter however here we explain how we incorporate reweighting when optimizing the objective function $\mathcal{L}'$ when a trajectory X has been obtained from a biased simulation. To see this is done suppose that as we ran a biased simulation and we record the trajectory $X = \{X_1, X_2, \cdots, X_{M+k}\}$ of the system. Suppose further that we also record the bias potential that the system experienced throughout this simulation, namely $V = \{V_1, V_2, \cdots, V_{M+k}\}$. Equipped with this information we can then apply the principle of importance sampling [24] to write our PIB objective function $\mathcal{L}'$ as,

$$\mathcal{L}' = \left\{ \sum_{n=1}^{M} e^{\beta V^n} \right\}^{-1} \sum_{n=1}^{M} e^{\beta V^n} \log Q(X_{n+k}|\chi_n), \tag{2.28}$$

where β is the inverse temperature. Now that we have all this information we are ready to work out an example.

Chapter 3

$2d$ Ising Model using pRAVE

In the following analysis pRAVE was used for enhanced sampling on the $2d$ Ising model where we set $\Delta t = 0$ such that $X_{\Delta t=0} = X$. This means that rather than using pRAVE to construct a PIB that allows us to predict future information about the system, we used pRAVE to construct a PIB that would allow us to reconstruct our input dataset X, (see Fig. 2.3).

3.1 Metropolis Rejection Algorithm

Throughout this chapter we will refer to an "MC sweep" as an attempt to update N randomly chosen lattice sites by making use of the Metropolis algorithm. To do this we will,

1. Compute the energy E_i of the current lattice configuration X_i.
2. Select a lattice site at random, flip the spin at this site, and set this to be our trial microstate X_t with a corresponding of energy E_t.
3. Compute the probability $p = \min(1, p_t/p_i)$ of making the transition from X_i to X_t, using a random number generator that generates a float c between 0 and 1. If $c < p$, then we will accept the trial microstate X_t to be our microstate X_{i+1}. If $c > p$, we will stay in our current lattice configuration, $X_{i+1} = X_i$

This will be done N times to complete one MC sweep and we will perform M MC sweeps in every simulation. Now that we have this dataset we can compute the order parameters that will be fed to pRAVE to compute the weights a, b, and c from the optimization of the objective function $\mathcal{L}'$.

3.2 Order Parameters and Reaction Coordinate

In order to construct a bias potential that can be use for enhanced sampling we first need to define what the order parameters of the reaction coordinate will be. This set of order parameters which will be computed at the end of every MC sweep will serve as our high dimensional data that will be mapped onto a low dimensional manifold, as explained in Sec. 2.4. The order parameters the we will be considering will be the average magnetic moment of the lattice configuration,

$$S_1 = \langle m \rangle = \frac{1}{N} \sum_{i=1} \sigma_i, \tag{3.1}$$

the average nearest neighbor interaction energy,

$$S_2 = -\frac{1}{4N} \sum_{i,j} \sigma_{i,j}(\sigma_{i,j+1} + \sigma_{i,j-1} + \sigma_{i+1,j} + \sigma_{i-1,j}), \tag{3.2}$$

and average second nearest neighbor interaction energy,

$$S_3 = -\frac{1}{16N} \sum_{i,j} \sigma_{i,j}(\sigma_{i,j+1} + \sigma_{i,j-1} + \sigma_{i+1,j} + \sigma_{i-1,j})(\sigma_{i+1,j+1} + \sigma_{i+1,j-1} + \sigma_{i-1,j+1} + \sigma_{i-1,j-1}), \tag{3.3}$$

where N is the number of lattice sites on the $L \times L$ square lattice. It is important to note here that using S_1 as our only order parameter would have been sufficient to construct a bias potential. The reason for this is that the magnetization alone captures both phases of the system, the ordered phase where the system remains trapped in a state with either positive or negative magnetizations at $T << T_C$, as well as the disordered phase at $T > T_C$ where the system makes frequent transitions back and forth between these two states. However, we also include the order parameters S_2 and S_3 so that we can see how the importance of these three order parameter varies as we increase the temperature T of the system. This will be demonstrated in a similar fashion as that proposed in Sec. 2.3, however, here we will compare the magnitude a, b, and c after the system has been successful in visiting a large portion of the energy landscape, as we will explain shortly. We will achieve this by running several iterations of biased MC simulations so that we sample as much of the energy landscape as possible. This way we can have increasing confidence that the parameters a, b, and c represent the parameters for reaction coordinate of our system at temperature T.

Now that we have defined the order parameters that we will be considering we can define our PIB which we define to be our reaction coordinate as mentioned at the end of Sec. 2.4. We now define our reaction

coordinate,

$$\chi = aS_1 + bS_2 + cS_3, \tag{3.4}$$

that will allow us bias the system by using a bias potential in running MC simulation. Now that we have defined the order parameters S_1, S_2, and S_3 and our reaction coordinate it is time to explain how we will construct the bias potential V_{bias}. At the end of every MC sweep the configuration of the lattice is recorded which allowed us to compute the order parameters defined in above. Since an MC simulation will be comprised of M MC sweeps, the trajectory X that we will using to determine the parameters a, b, and c that optimize $\mathcal{L}'$ will be of size $3 \times M$. Every time pRAVE modifies the parameters for all the neurons of deep neural network in process of optimizing $\mathcal{L}'$ will be referred to as an "epoch". pRAVE will perform 10^4 epochs for each dataset X. At the end of every epoch, the neural network will compute the mean squared error (MSE) to let us know how the pRAVE is performing in the optimization from which we can make plots to determine whether we can trust the parameters a, b, and c that pRAVE found to optimize $\mathcal{L}'$. An example of such a plot is demonstrates in Fig. 3.1,

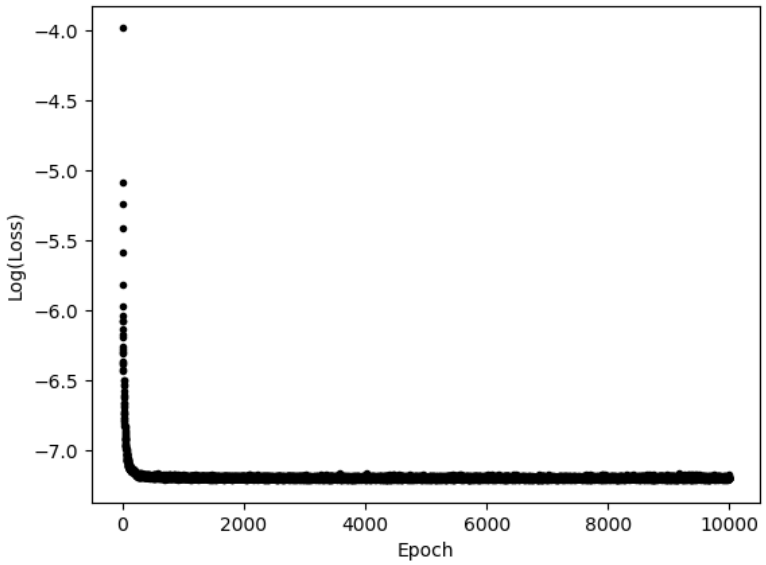

Figure 3.1: Plot of the log(loss) = log(MSE) vs. Epoch, that pRAVE measured at the end of every epoch.

pRAVE also records the values of the weights a, b, and c at the end of every epoch in the optimization of our objective function (see Fig. 3.2). This allows us to see if the weights a, b, and c have converged to weights we can use to construct the reaction coordinate or if we need to increase the number of epochs that pRAVE needs to perform to converge to values a, b, and c that optimize the objective function $\mathcal{L}'$.

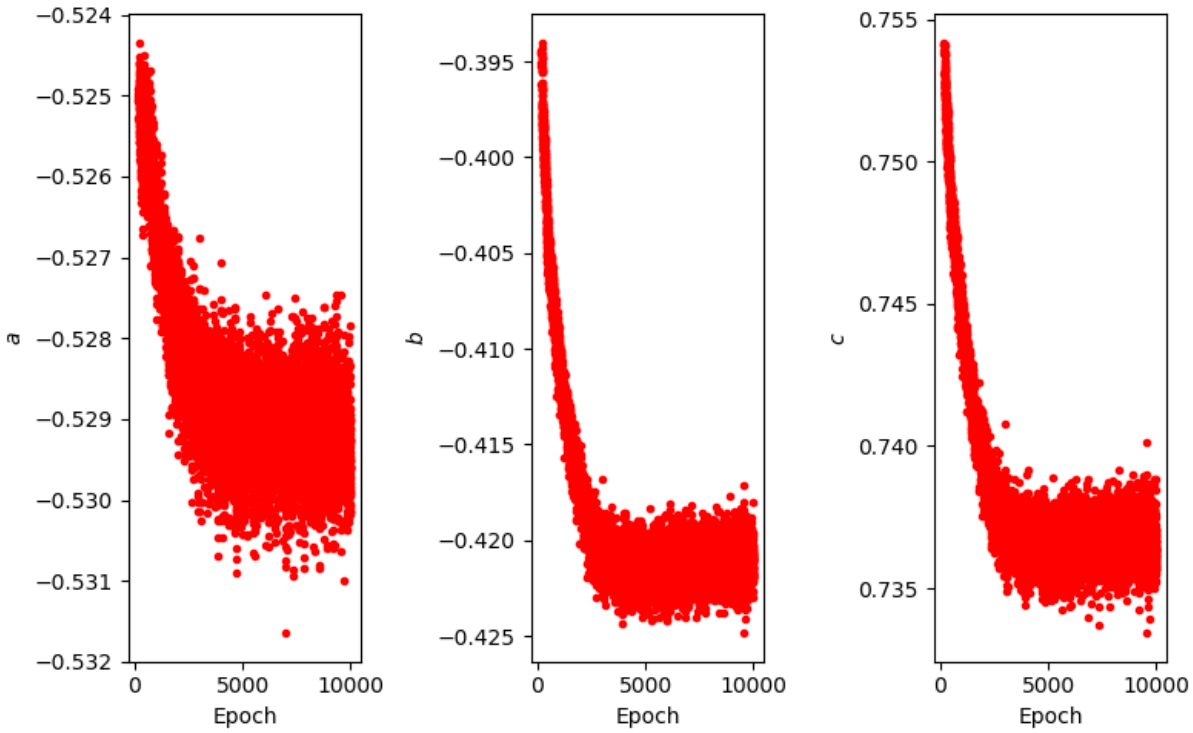

Figure 3.2: Weights a, b, and c used to construct the reaction coordinate $\chi = aS_1 + bS_2 + cS_3$ after 10^4 epoch.

3.3 Constructing the Bias Potential

After mapping our trajectory X onto χ we can construct a normalized histogram with our data χ. The histogram will range from χ_{min} to χ_{max} and will have a bin width of $\Delta\chi$. The probability distribution with respect to χ will then be given by,

$$P^u(\chi) = \langle \delta(\chi - \chi(t)) \rangle, \tag{3.5}$$

where the superscript u is used to denote that we have constructed the probability distribution using an unbiased trajectory. We can then construct a bias potential $V_{bias}(\chi)$ using,

$$V_{bias}(\chi) = k_B T \ln P^u(\chi) = k_B T \ln \langle \delta(\chi - \chi(t)) \rangle, \tag{3.6}$$

such as the bias potential plotted in Fig. 3.3.

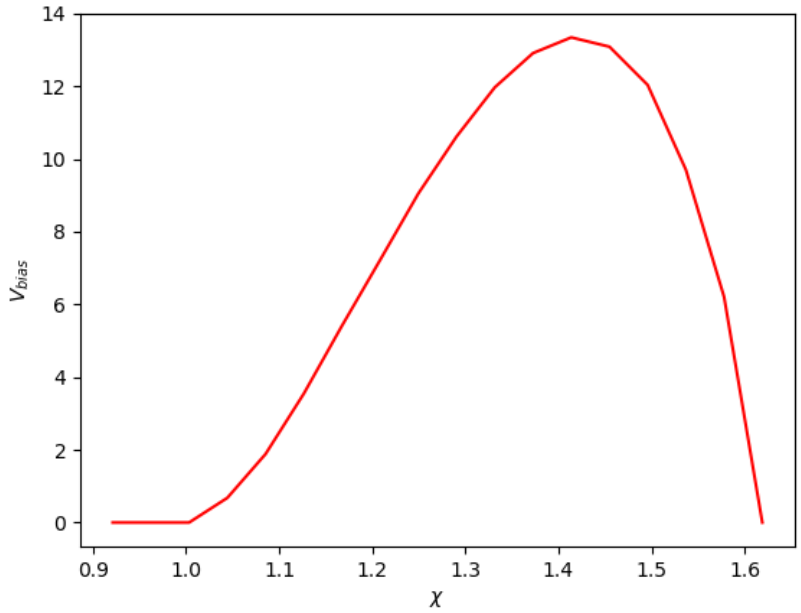

Figure 3.3: V_{bias} (is in units of k_BT) constructed from the unbiased MC simulation data in Fig. 3.7 where the system remain trapped in the state with negative average magnetic moments.

Since this bias potential will be largest for reaction coordinate values that were frequently visited, applying this bias potential to the next MC simulation will encourage the system to visit microstates corresponding to reaction coordinate values that were not frequently visited. The way that we will incorporate this bias potential in our simulations is this: Suppose after initializing our lattice we are in the microstate X_i with energy E_i and corresponding reaction coordinate value χ_i. We will assign a corresponding $V_{bias}(\chi_i)$ to this microstate by interpolating. Next we will select a lattice site at random, flip this spin, and set this to be our trial microstate X_t. We will then compute the energy E_t and corresponding bias $V_{bias}(\chi_t)$ for this microstate. The probability of going from microstate X_i to X_t in this biased simulation will then be

$$p = \min\ (1, p_t/p_i) = \min\ (1, \exp\{-\beta(\Delta E + \Delta V_{bias})\}). \tag{3.7}$$

Similar to what we've done in unbiased simulations, we will use a random number generator to generate a float c between 0 and 1. We will set X_{i+1} to X_t if $c < p$ and X_{i+1} to X_i if $c > p$.

As mentioned at the end of Sec. 2.4, all simulations that we run with a bias potential will be under the influence of this potential that has been added to the original Hamiltonian, we will therefore have to reweight the trajectory to account for this. This is achieved by multiplying each data point $X_i \in X$, with

reaction coordinate value $\chi_i \in \chi$, by using the following weight,

$$w_i = e^{\beta V_{bias}(\chi_i)}, \tag{3.8}$$

that depends on the amount of bias that we applied to the system during the biased MC simulation. This also allows us to obtain an unbiased probability distribution from a biased trajectory by using,

$$P^u(\chi) = \frac{\langle w\delta(\chi - \chi(t))\rangle_b}{\langle w\rangle_b} \tag{3.9}$$

which we can use to construct a bias potential for further rounds of biased MC simulations using Eq. 3.6.

3.4 Results

3.4.1 Reaction Coordinate

The weights a, b, and c that we have obtained through successive biased simulations at temperature T until the free energy surfaces have converged are listed below in Table 3.1 and are plotted in Fig. 3.4. For temperatures $T > 0.99T_C$ we used the converged weights from our analysis at $T = 0.99T_C$. We did this because looking at the plot in Fig. 3.4 we see that weights do not change appreciably.

T/T_C	a	b	c
0.9	-0.5021	-0.4161	0.7581
0.925	-0.5316	-0.3795	0.7572
0.95	0.6369	0.0172	-0.7706
0.97	-0.6122	0.0327	0.7900
0.99	-0.6409	0.0146	0.7674

Table 3.1: Weights a, b, and c for the reaction coordinate $\chi = aS_1 + bS_2 + cS_3$, at various temperatures.

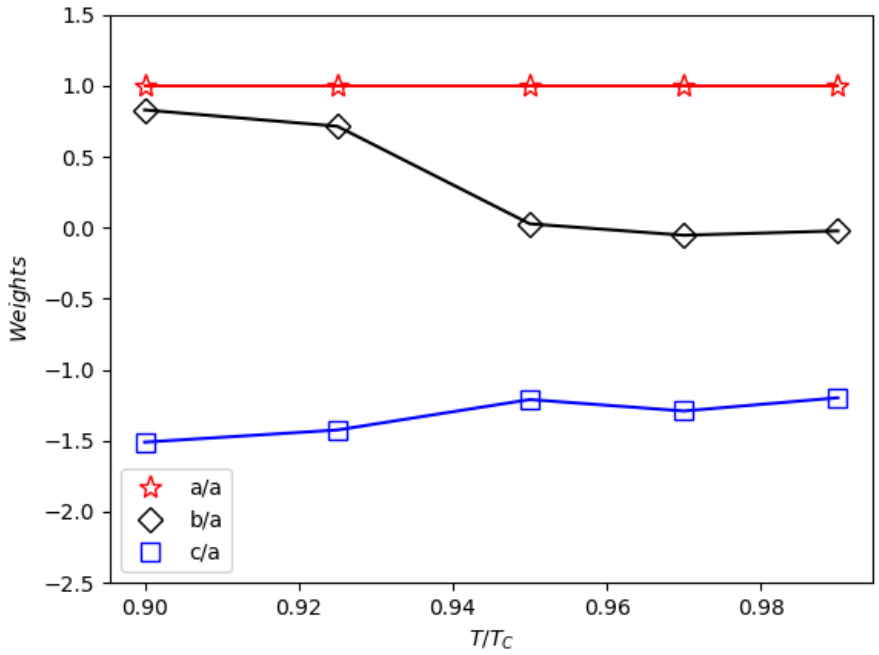

Figure 3.4: Plotted are the weights from Table 3.1 where we have normalized weights b and c by the value of a at each of the indicated temperatures.

These weights in Table 3.1 were obtained by running several rounds of biased simulations until the basins of the energy landscape for the system were filled by the bias potential we have constructed. A signature for when this occurs is when we observe rapid transitions between positive and negative average magnetic moment states as shown in Fig. 3.5. Another signature telling us that we have filled the basins of the energy landscape is obtained by plotting $\log P$ as in Fig. 3.6, where P is the un-reweighted trajectory along the reaction coordinate χ. By observing this plot to be approximately flat along χ tells us that the system visited all reaction coordinates χ_i just as frequent which is what this enhanced sampling method set out to achieve.

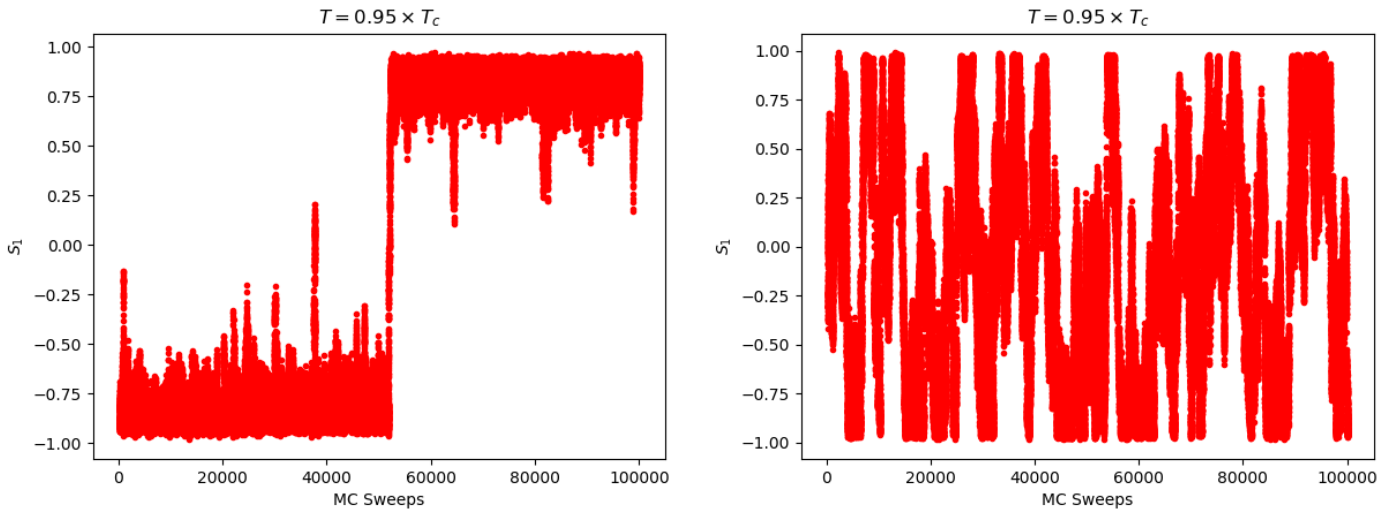

Figure 3.5: (Left) Trajectory of the system when running an unbiased simulation for 10^5 MC Sweeps. (Right) Trajectory of the third biased MC simulation after running a simulation for 10^5 MC Sweeps. The system on the right is under the influence of a bias potential that was constructed from the trajectory of the second biased MC simulation.

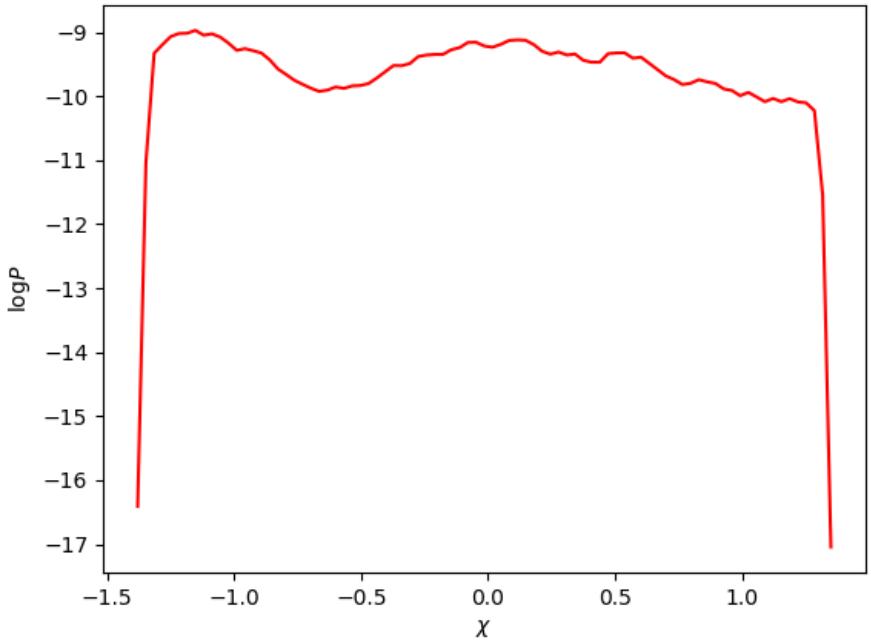

Figure 3.6: log of the normalized histogram that was constructed by mapping the trajectory on the right of Fig. 3.5 onto the reaction coordinate χ. The approximate flatness of the histogram tells us that basins of the energy landscape are nearly filled.

3.4.2 Improved Sampling Through pRAVE

Here we illustrate how enhanced sampling allowed us to explore the energy landscape by using successive rounds of biased MC simulations which allowed us to determine the weights a, b, and c from the previous section. In Fig. 3.8 we see the trajectory for an unbiased simulation at temperature $T = 0.9T_C$ where the system remained tapped in a state with positive average magnetizations, $S_1 = \langle m \rangle$.

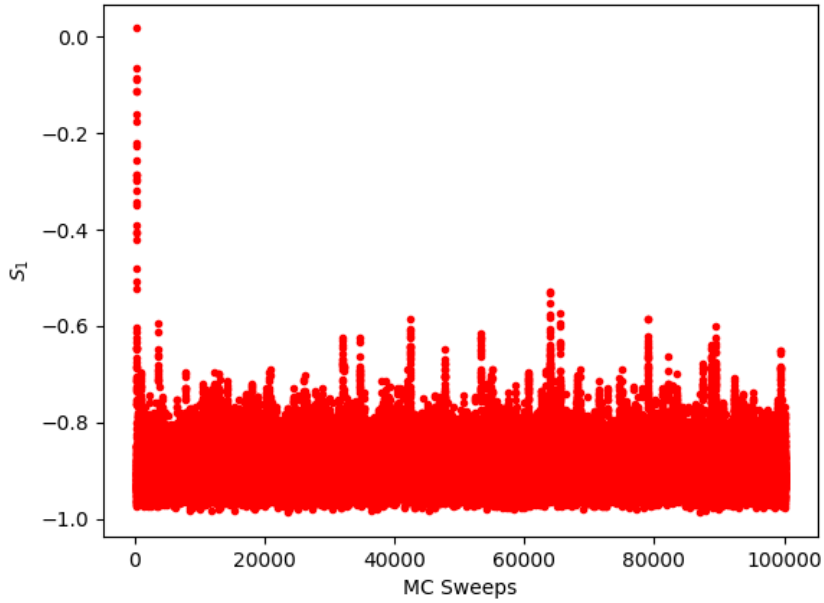

Figure 3.7: Trajectory of an unbiased MC simulation at $T = 0.9T_C$ where the system has transitioned into a state with negative average magnetic moments and remained trapped in.

Using the data from this trajectory we were able to construct the bias potential shown in Fig. 3.8. This bias potential was then used in the first biased MC simulation producing the trajectory plotted in Fig. 3.9. From Fig. 3.9 we see that the system has been able to explore more of the energy landscape, which was the goal of this enhanced sampling method. Using this biased trajectory when can then perform reweighting to obtain a new set of weights using pRAVE that capture important information about this trajectory and that we can use to construct a bias potential for the second biased simulation. The bias potential that was used for the first biased simulation, $k_BT \ln P$, and $k_BT \ln P^u$ are all plotted in Fig. 3.10. Here P is the normalized trajectory along the new reaction coordinate χ without reweighting and P^u is the normalized trajectory along the new reaction coordinate χ with reweighting.

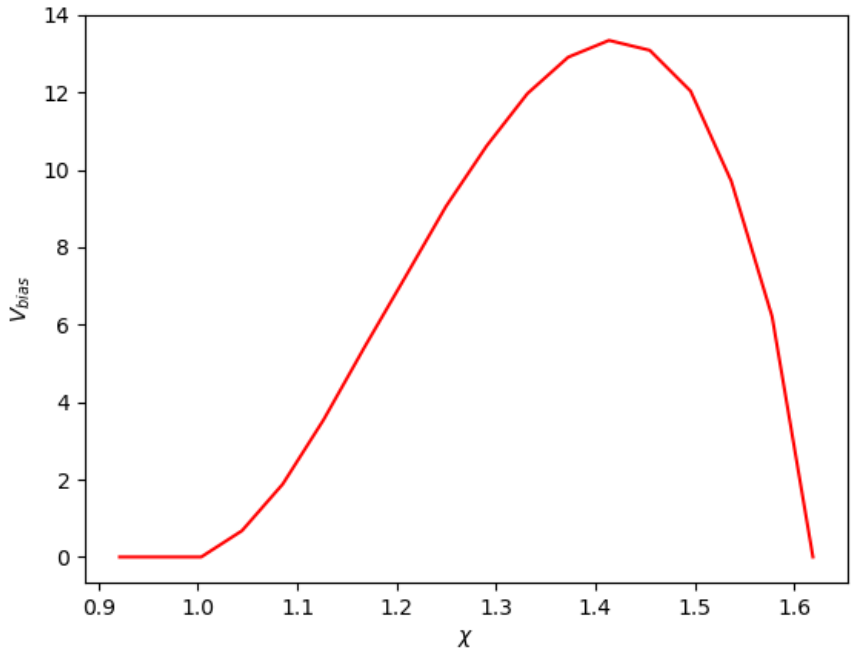

Figure 3.8: V_{bias} (is in units of k_BT) constructed from the unbiased MC simulation data in Fig. 3.7.

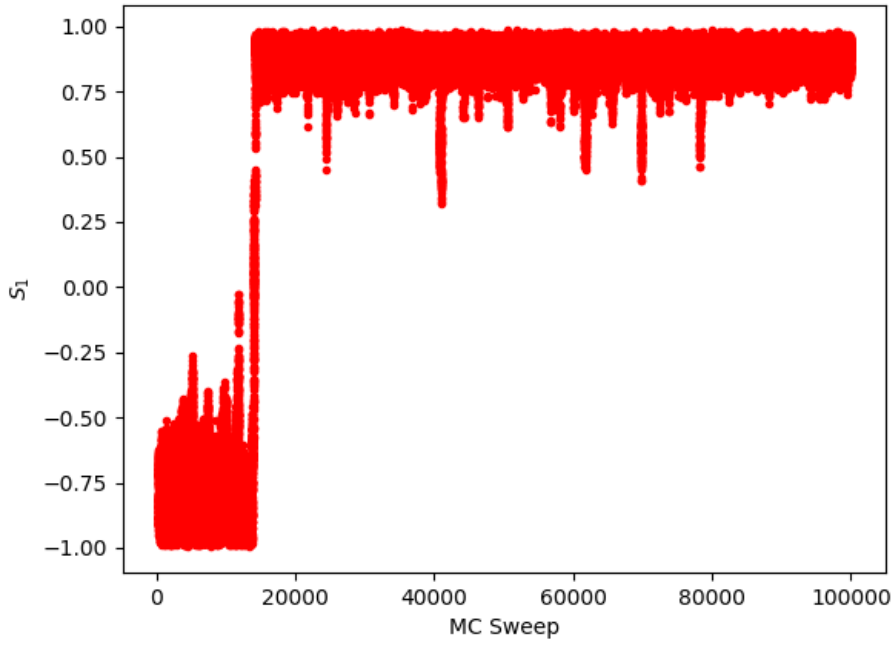

Figure 3.9: First biased MC simulation at $T = 0.9T_C$ where we see the system transitioning from the state with negative average magnetic moment to the state with positive average magnetic moment.

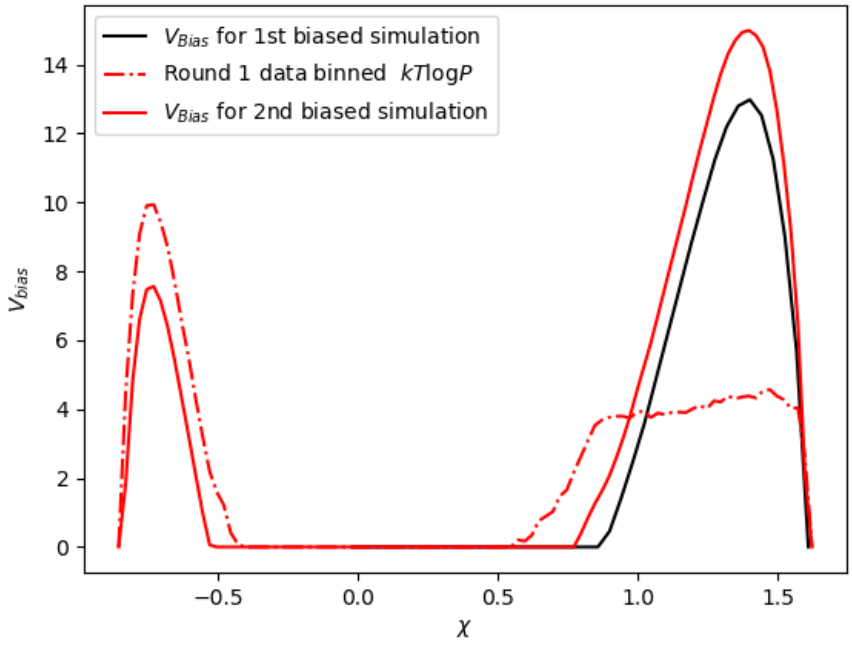

Figure 3.10: Here we see the effect of the bias potential (solid black curve). The system transitioned from a state with negative average magnetic moment to a state with positive average magnetic moment where the system remained trapped in (see Fig. 3.9) (dashed red curve). We also see the effect of reweighting the data (solid red curve).

We continue this process of running biased simulations until the bias potentials that we construct fill the basins of the energy landscape as mentioned at the end of the previous section. Once we have filled the energy basins we can compute the thermodynamics using the trajectory of our last biased MC simulation which we now discuss.

3.4.3 Thermodynamic Observables

In Fig. 3.6 we have plotted the free energy,

$$F(\chi_i) = -k_B T \ln Z_i, \tag{3.10}$$

where the subscript on the partition function is used to denote the partition function for a particular reaction coordinate value χ_i which is given by,

$$Z_i = \sum_{j \in \chi_i} e^{-\beta E_j}. \tag{3.11}$$

From this figure we can see that the height of the barrier separating the two states decreases as the temperature of the system increases. This is a result that we expected to observe [13] which is a good signature that our simulations of the system are working properly. In this figure we also see a shift of the free energy curves which is attributed to the large change in the magnitude of the weights from $T < 0.925T_C$ to $T > 0.925T_C$ that we see in Fig. 3.4.

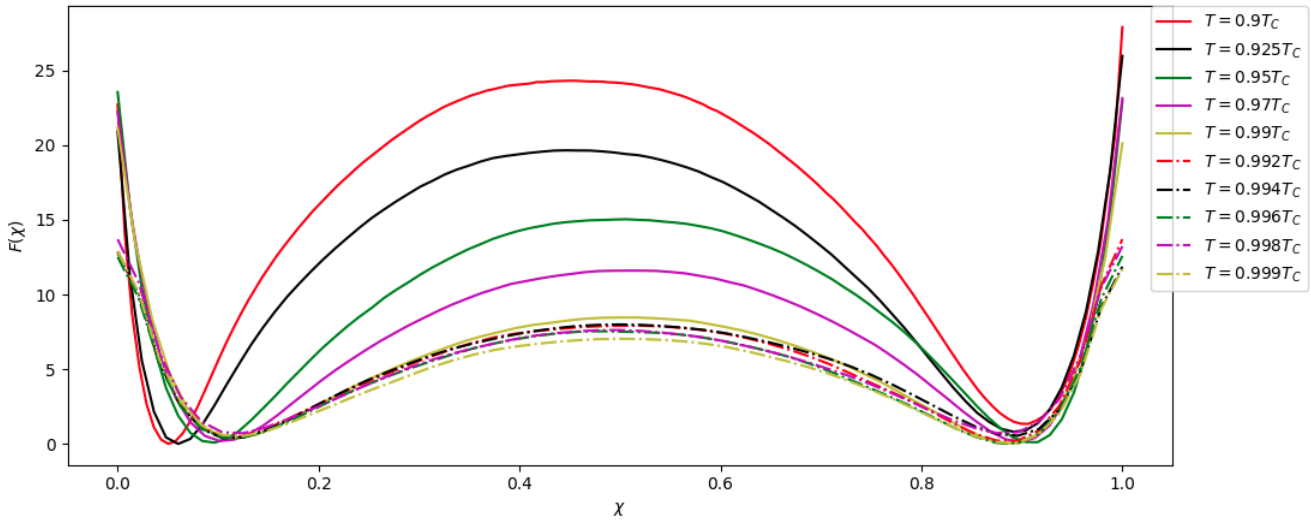

Figure 3.11: Free energy surfaces after several biased MC simulations. These surfaces were used to compute the partition function and from this the Gibbs free energy discussed in Sec. 3.4.3.

Given that we have information to compute $F(\chi_i)$ vs. χ as well as the trajectory of the last biased simulations at various values of T. We can use this information to compute the heat capacity C two different ways that will allow us to compare our numerical results to Onsager's result

$$C \sim -\left(\frac{8k_B N}{\pi}\right)(\beta J)^2 \ln|T - T_C|, \tag{3.12}$$

near the critical temperature. The first method will consist of computing the free energy of the system at various values of T. By fitting this data to an nth order polynomial we can take successive derivatives to get the entropy,

$$S = -\frac{\partial F}{\partial T}, \tag{3.13}$$

and the heat capacity,

$$C = -T\left(\frac{\partial^2 F}{\partial T^2}\right), \tag{3.14}$$

where F is the free energy of the system, Eq. 3.20. There is no distinction here as to whether we call the free energy here a Gibbs free energy or a Helmholtz free energy since pressure and volume are not relevant in

this lattice system. For this reason we omit the subscripts on the derivative of the heat capacity, Eq. 3.14.

The second approach to compute the heat capacity C for this Ising model makes use of computing the heat capacity from a statistical mechanics approach. To see this recall that the heat capacity can be written in terms of the fluctuations of $\langle E \rangle$, namely,

$$C = \frac{1}{k_B T^2}[\langle E^2 \rangle - \langle E \rangle^2], \tag{3.15}$$

where

$$\langle E \rangle = \frac{1}{Z} \sum_i E_i e^{-\beta E_i}, \tag{3.16}$$

and,

$$\langle E \rangle = \frac{1}{Z} \sum_i E_i^2 e^{-\beta E_i}. \tag{3.17}$$

However by making use of the ergodic hypothesis [13] we can convert Eq. 3.16 and 3.17 into Eq. 3.18 and 3.19 respectively.

$$\langle E \rangle = \frac{\sum_i E_i w_i}{\sum_i w_i} \tag{3.18}$$

and similarly,

$$\langle E^2 \rangle = \frac{\sum_i E_i^2 w_i}{\sum_i w_i}. \tag{3.19}$$

Both of these averages, Eq. 3.18 and 3.19, are easy compute since E_i is the ith average nearest neighbor interaction energy $S_{2,i}$ by construction. Also, $w_i = e^{\beta V_{bias}(\chi_i)}$, which is the associated to the ith S_2 data point.

Computing C Using the Gibbs Free Energy F

To compute the Gibbs free energy,

$$F = -k_B T \ln Z \tag{3.20}$$

where F is the Gibbs free energy of the system at temperature T, we sum over the free energies $F(\chi_i)$ in the partition function,

$$Z = \sum_i \exp\{-\beta F(\chi_i)\}. \tag{3.21}$$

Using these values we can then fit out F vs. T data to a 3rd degree polynomial to compute the entropy and heat capacity using Eq. 3.13 and 3.14 respectively. We chose to use a 3rd order polynomial since we will have to take a second order derivative of our fitted curve to compute C. If we were to choose a degree of one

or two we would have a constant heat capacity for all temperatures, which we know we should not observe. We also do not want to over fit the data by using a high degree polynomial. These are the reasons why we chose to use a 3rd degree polynomial. Plots for the Gibbs' free energy, entropy, and heat capacity computed using this method are plotted in Fig. 3.12, 3.13 and 3.14 respectively.

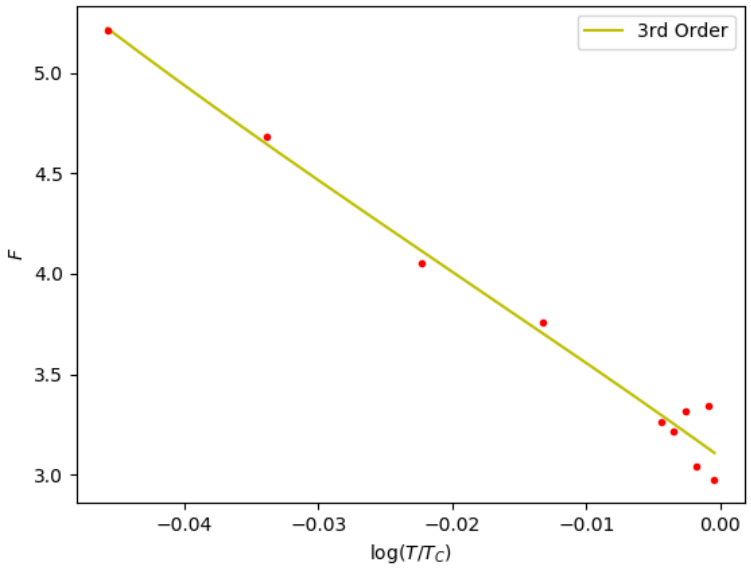

Figure 3.12: F vs. $\log_{10}(T/T_C)$

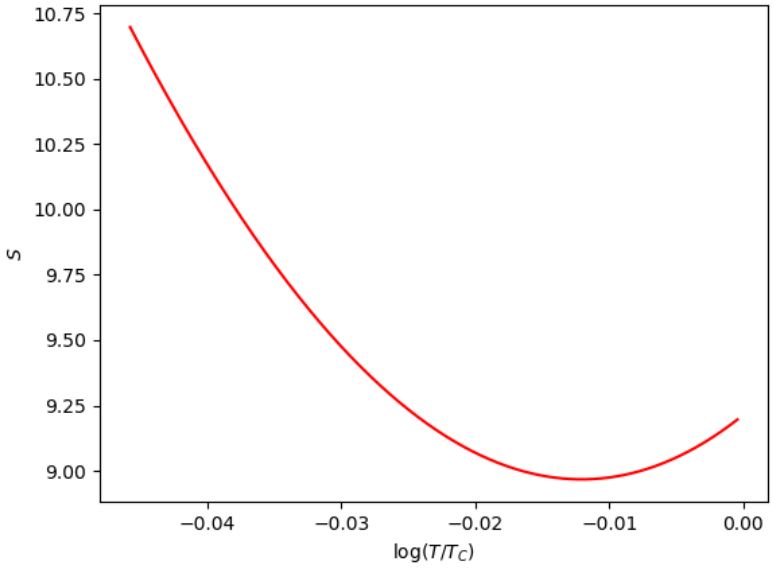

Figure 3.13: S vs. $\log_{10}(T/T_C)$

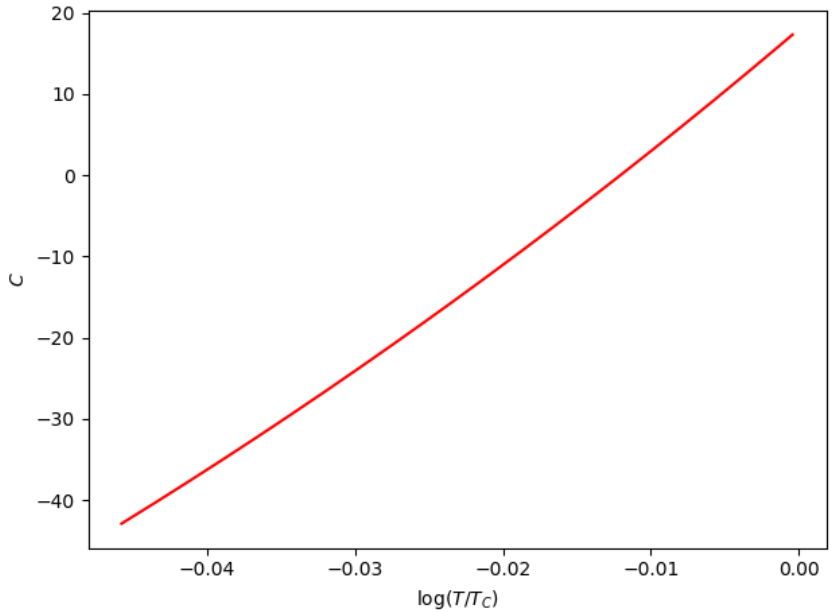

Figure 3.14: C vs. $\log_{10}(T/T_C)$

From the heat capacity plot in Fig. 3.14 we see that we have negative heat capacity at a wide range of temperatures, a result that is nonphysical for this system. This negative heat capacity arose from the multiplicative coefficients that were used to fit the F vs. T data to the 3rd order polynomial. From the fitting we obtain,

$$F = aT^3 + bT^2 + cT + d, \tag{3.22}$$

such that

$$C = -6aT^2 - 2bT. \tag{3.23}$$

Since $T > 1$ we have that we will we have negative C values if both $a, b > 0$ or if $b < 0$ and $a > 0$. However, there is not way of knowing whether we will obtain negative C values until the fit is performed. To overcome this issue with fitting we make use of Eq. 3.15 which is guaranteed to be positive due to the nature of the variance and unlike the fitting approach was derived using a more rigorous and physical approach. The values for Eq. 3.15, 3.18, and 3.19 are listed in Table 3.2 and are plotted against Onsager's results in Fig. 3.15.

T/T_C	$\langle E \rangle$	$\langle E^2 \rangle$	C
0.900	-0.857	0.735	3.24×10^{-4}
0.925	-0.832	0.693	3.84×10^{-4}
0.950	-0.802	0.645	4.64×10^{-4}
0.970	-0.773	0.600	5.54×10^{-4}
0.990	-0.739	0.549	6.56×10^{-4}
0.992	-0.734	0.542	6.63×10^{-4}
0.994	-0.732	0.540	6.63×10^{-4}
0.996	-0.728	0.533	6.74×10^{-4}
0.998	-0.723	0.526	6.81×10^{-4}
0.999	-0.722	0.524	6.89×10^{-4}

Table 3.2: Thermodynamic observables computed at various temperatures.

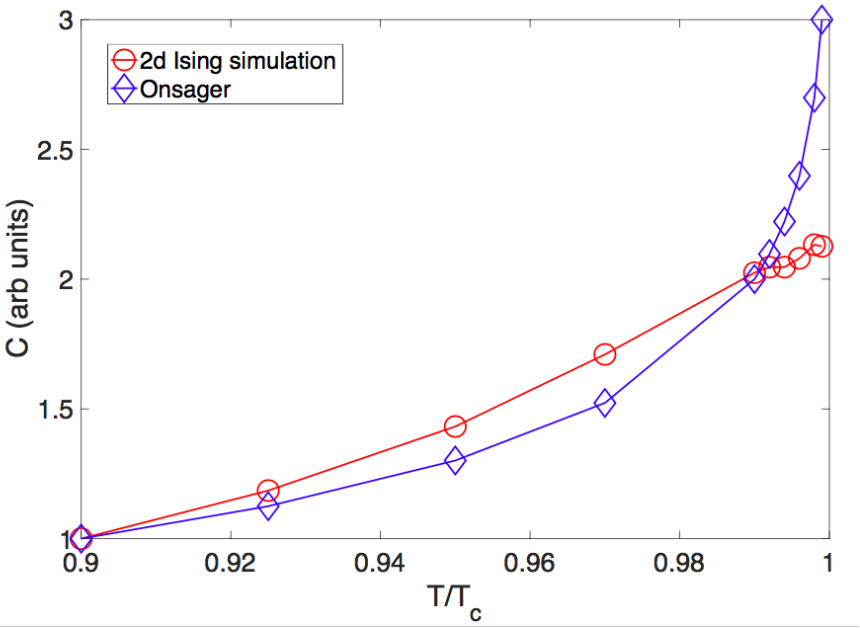

Figure 3.15: Onsager's heat capacity curve and our numerical results at various temperatures.

From Fig. 3.15 we see an agreement in our capacity calculations compared to Onsager's results at temperatures below $0.99T_C$. However, as the critical temperature is approached our numerical results do not show the divergence of the heat capacity that we would expect. The reason for this might be due to the fact that we need to do more sampling at these temperatures or the fact that the lattice that we used to perform this analysis was a 25×25 lattice with 625 lattice sites while Onsager's analysis was done for a lattice where $N \to \infty$.

Chapter 4

Conclusion and Outlook

As mentioned in Ch. 3, the trend that we observed where the energy barrier in the free energy plots decrease as the temperature increases was in agreement with what we should expect. This is a signature that our simulations are working properly. Our results for the heat capacity at temperatures below $T = 0.99T_C$ were also in agreement with Onsager's asymptotic solution near the critical temperature, Eq. 3.12. However, due to the small lattice that was used in this analysis, 25×25 lattice with $N = 625$ lattice sites, we were not able to capture the divergent behavior of the heat capacity at temperatures above $T = 0.99T_C$. For this reason, analysis will be done using larger lattices, e.g. a lattice of size 50×50 with $N = 2,500$ lattice sites. This will allow us to study the accuracy of our method as a function of the lattice size, which we expect to become more accurate as $N \to \infty$. We can also perform an analysis similar to what was done in this thesis to compute the renormalized coupling constants similar to what was done in [12]. By performing such an analysis we will be able to compare the analysis of pRAVe against the variational approach in [12].

As mentioned at the beginning of Ch. 3, this analysis was performed with $X_{\Delta t=0}$ such that pRAVE was used to reconstruct the input data X using the PIB χ. One thing that we can explore is pRAVE's performance in constructing a PIB when we increase the values of Δt, thereby exploring the full potential of pRAVE. Performing this analysis by using an increasing value of Δt should allow us to obtain the same weights a, b, and c using fewer rounds of biased simulations, thereby reducing the amount of computational resources needed to perform analyis similar to what was done here.

The analysis in this thesis was performed on the simple $2d$ Ising model without an external magnetic field, Eq. 1.1. However, pRAVE can easily be generalized to consider lattice models such as, the $2d$ Ising

model in the presence of an external magnetic field,

$$H = -J \sum_{i,j} \sigma_{i,j}[\sigma_{i+1,j} + \sigma_{i-1,j} + \sigma_{i,j+1} + \sigma_{i,j-1}] + h \sum_{i,j} \sigma_{i,j}, \tag{4.1}$$

as was explored in [26] to study the competing effect of a growing nucleus. We can perform an analysis similar to theirs to compare our methods performance. We can also explore more complicated lattice models where we consider various coupling constants such as in the following Hamiltonian,

$$H = -J_1 \sum_{i,j} S_i^1 \cdot S_j^1 - J_2 \sum_{i,j} S_i^2 \cdot S_j^2 - J_{12} \sum_{i,j} S_i^1 \cdot S_i^1, \tag{4.2}$$

where the values of J_1, J_2, and J_{12} modulate the physics of the lattice and allow us to explore how they affect nucleation mechanisms, similar to that was done in [26]. Exploring complex $3d$ Hamiltonians will also allow us to study phase transitions in $3d$ lattice models which is an active field of study. We can then study how various order parameters change as the critical point is approached, thereby allowing us to explore the dynamics of the system leading up to the phase transition.

Bibliography

[1] Ribeiro, J. M. L. et al., *Reweighted Autoencoded Variational Bayes for Enhanced Sampling (RAVE)*. May 4, 2018. J. Chem. Phys. 149, 072301.

[2] Bussi G., Laio A., Tiwary P. , *Metadynamics: a unified framework for accelerating rare events and sampling thermodynamics and kinetics.* Handbook of Materials Modeling (Springer), Ed. Sidney Yip and Wanda Andreoni, 2018

[3] Tiwary, P., Berne, B. J., *Spectral gap optimization of order parameters for sampling complex molecular systems*. Jan. 20, 2016 PNAS. 113 (11) 2839-2844

[4] Valsson O., Parrinello M., *A Variational Approach to Enhanced Sampling and Free Energy Calculations*. Aug. 27, 2014. Phys. Rev. Lett. 113, 090601.

[5] Wang, Y. et al., *Past–future information bottleneck framework for simultaneously sampling biomolecular reaction coordinate, thermodynamics and kinetics*. Dec, 28, 2018. BioRxiv preprint

[6] Berg, B. A., *A brief history of the introduction of generalized ensembles to Markov chain Monte Carlo simulations*. April 5, 2017. Eur. Phys. J. Special Topics 226, 551–565

[7] Murthy K. P. N., *Metropolis and Wang-Landau Algorithms*. Sept. 27, 2017. arXiv preprint 1709.09352

[8] Metropolis et al., *Equation of State Calculations by Fast Computing Machines*. June 1953. J. Chem. Phys. 21, 1087

[9] Liang, F., Wong, W. H., *Evolutionary Monte Carlo for Protein Folding Simulations*. Aug. 6, 2001. J. Chem. Phys. 115, 3374

[10] Frenkel, D., Smit, B., *Understanding Molecular Simulation: From Algorithms to Applications, Vol 1*. Academic Press, Orlando, FL. 2001

[11] Kadanoff, L. P.. *Scaling Law for Ising Model Near T_C*. June 1966. Physics 2, 263.

[12] Wu Y., Car R., *Variational Approach to Monte Carlo Renormalization Group*. Nov. 28, 2017. Phys. Rev. Lett. 119, 220602

[13] Chandler, D., *Introduction to Modern Statistical Mechanics*. Oxford, New York, New York, 1987.

[14] Schwabl, F. *Statistical Mechanics*. Springer, Berlin, Germany, 2006.

[15] Wilson K. G., *Renormalization Group and Critical Phenomena. I. Renormalization Group and the Kadanoff Scaling Picture*. Nov. 1, 1971. Phys. Rev. B 4, 3174

[16] Swendsen R. H., *Monte Carlo Renormalization Group*. April 2, 1979. Phys. Rev. Lett. 42, 859

[17] Landau, D. P., Tsai, S. H., Exler, M., *A new approach to Monte Carlo simulations in statistical physics: Wang-Landau sampling*. Sept. 13, 2004. American Journal of Physics 72, 1294

[18] Goodfellow, I., Bengio, Y., Courville A., *Deep learning*. MIT Press. 2016.

[19] Onsager, L., *Crystal Statistics. I. A Two-Dimensional Model with an Order-Disorder Transition*. Phys. Feb. 1, 1944. Rev. 65, 117.

[20] Tishby, N., Pereira, F. C., Bialek, W. , *The information bottleneck method*. April 24, 2000. arXiv preprint physics/0004057

[21] Still S., *Information Bottleneck Approach to Predictive Inference*. Feb. 17, 2014 Entropy. 16, 968-989

[22] Nauenberg, M., Nienhuis, B., *Renormalization-Group Approach to the Solution of General Ising Models*. Dec. 30, 1974. Phys. Rev. Lett. 33, 1598.

[23] Zhou, C., Su, J., *Optimal modification factor and convergence of the Wang-Landau algorithm*. Oct. 20, 2008. Phys. Rev. 78, 046705

[24] Valsson, O., Tiwary, P., Parrinello, M.. *Enhancing Important Fluctuations: Rare Events and Metadynamics from a Conceptual Viewpoint*. March 10, 2016. Annu. Rev. Phys. Chem. 67:159–84

[25] MacKay, D. J. C., *Information Theory, Inference, and Learning Algorithms*. Cambridge University Press. 2003

[26] Pan, A. C., Chandler, D., *Dynamics of Nucleation in the Ising Model*. Sept. 28, 2004 J. Phys. Chem. 108, 51, 19681-19686

[27] Tiwary, P., et al., *Kinetics of protein–ligand unbinding: Predicting pathways, rates, and rate-limiting steps*. Feb. 3, 2015. PNAS. 112 (5) E386-E391

[28] Larsen, K. L.,*Dynamics of Nucleation in the Ising Model*. Oct. 28, 2011. Science. Vol. 334, Issue 6055, pp. 517-520